Annals of Nuclear Energy 146 (2020) 107616

Contents lists available at ScienceDirect

Annals of Nuclear Energy

journal homepage: www.elsevier.com/locate/anucene

Subchannel analysis of annular fuel assembly using the preconditioned Jacobian-free Newton Krylov methods

H. Esmaili *, H. Kazeminejad, H. Khalafi, S.M. Mirvakili

Nuclear Science and Technology Research Institute (NSTRI), P.O. Box 11365-3486, Tehran, Iran

ARTICLE INFO

Article history:
Received 16 February 2020
Received in revised form 27 April 2020
Accepted 25 May 2020
Available online 9 June 2020

Keywords:
Subchannel annular fuel
Newton-Krylov methods
Drift Flux Model
Preconditioning

ABSTRACT

In this paper, a numerical procedure for thermal–hydraulic subchannel analysis of the annular fuel assembly in a PWR using the drift-flux model (DFM) is presented. The system of nonlinear equations was solved with a fully-implicit solution scheme using the Jacobian-free Newton-Krylov (JFNK) method. To improve the computational efficiency and numerical stability of the JFNK method, a semi-implicit physics-based preconditioner was implemented. To validate the present method, various annular fuel arrays with different operating conditions were modeled, and the results were compared with the results of other codes. The key thermal–hydraulic parameters were in good agreement and the difference in total pressure drop values obtained by different methods was less than 2%. Also, it was found that the departure from nucleate boiling ratio (DNBR) of the outer channel was significantly larger than the inner channel, and the heat split ratio of the inner surface to the outer surface was approximately 1.4.

1. Introduction

The energy produced by the nuclear power plants is one of the most important sources of energy supply in the world. Currently, this energy is generated by the fission within nuclear reactors. Dual-cooled annular fuels have been proposed as an alternative to the conventional solid fuels to improve the power density by 50% while maintaining sufficient safety margins, Hejzlar et al. (2001) and Feng et al. (2007). Due to the benefits of this type of fuel, there has been much research in the use of annular fuels. Part of this research has focused on neutron discussions (Xu et al., 2007), and some on thermal–hydraulic issues (Han and Chang, 2003; Feng et al., 2007; Shin et al., 2012) and some on thermo-mechanics (Yuan, 2004; Deng et al., 2016).

In 2007, Feng et al. (2007) modified the VIPRE-01 code to investigate the thermal–hydraulic performance of annular fuels for the Westinghouse reactor with a power of 3411 Wt. In this study, different arrays (from 11 × 11 to 15 × 15) of annular fuels were investigated, which in some arrays (13 × 13) have the potential to increase the power up to 50%. In Korea, extensive research has been carried out on the use of annular fuels in the OPR-1000 light water reactors (Shin et al., 2012). Han and Chang (2003) developed the Thermal-Hydraulic analysis code for Annular Fuel (THAF) code coupled with MATRA code to analyze the thermal–hydraulic of the annular fuels. In recent years, to expand the use of annular fuels in India's new generation heavy water reactors, Vishnoi et al. (2012), Deokule et al. (2014,2015) have investigated the use of annular fuels in advanced heavy water reactors. In these studies, they have developed SAAP (Sub-channel Analysis of Annular Pin bundle) software. This software also runs using COBRA-IV-I software.

Current subchannel analysis codes such as COBRA-EN (Basile et al., 1999), MATRA (Yoo et al., 1999), and VIPRE-01 (Stewart et al., 1983) are not capable of modeling annular fuel assembly. Computationally, the distribution of heat and fluid flow into the internal and external channels is unknown, because one of the most critical issues in the thermo-hydraulic analysis of annular fuels is to find the amount of internal and external fluid flow and heat split between the internal and external channels. The computational methods implemented in these codes are also computationally expensive. Hence, more accurate methods with less computational cost are needed, and the researches to develop a subchannel code with annular fuel modeling capability have been continued.

In the most recent study, Xia et al. (2019) developed a Subchannel Analysis Code for Annular Fuel (SACAF) capable of thermo-hydraulic modeling of annular fuels. In this study, the homogeneous flow model was applied for two-phase flow modeling, also the closed channel model is used to define the internal channels, and the open channel model is used to define the external channels. In this paper, the finite difference method is applied to solve the mass, momentum, and energy equations.

* Corresponding author.
E-mail address: hesmaeili@aeoi.org.ir (H. Esmaili).

https://doi.org/10.1016/j.anucene.2020.107616
0306-4549/

Nomenclature

Latin characters

A	flow area (m^2)
C_0	distribution parameter
D	diameter (m)
f	friction coefficient
F	residuals/residual vector
G	mass flux, [kg/m^2s]
g	gravitational acceleration (m/s^2)
h	enthalpy (J/kg)
H_{ig}	liquid–vapor interfacial heat transfer coefficient (W/K)
J	Jacobian matrix
K	form loss factor (–)
L_c	gap lateral length (m)
P	Pressure (Pa)
P	preconditioning matrix
q“	heat flux (w/m^2)
Re	Reynolds number
s_{ik}	channel gap (m)
t	time (s)
T	Temperature (K)
u	velocity (m/s)
V_{gj}	drift velocity of gas phase (m/s)
$\overline{V_{gj}}$	mean drift velocity of gas phase (m/s)
w'_{ik}	cross flow from channel-i to channel-k per unit axial length [kg/(m.s)]
w'_{ik}	diversion cross flow from channel-i to channel-j per unit axial length[kg/(m.s)]
x	unknown vector
z	axial coordinate (m)

Greek symbols

α	void fraction
δ	differencing operator (–)
σ	surface tension, (N/m)
Δ	differencing operator (–)
Δt	time step (s)
Δz	spatial step (m)
ρ	density (kg/m^3)
Γ	volumetric vapor generation rate, (kg/m^3s)
ξ	heated perimeter (m)

Subscripts

l	Liquid phase
w	wall
g	saturation vapor
f	saturation liquid
sat	saturation condition
m	mixture
n	fuel number
i	channel number
j	mass and energy control volume
j ± 1/2	momentum control volume
k	Adjacent Sub-channel to sub-channel-i

Superscripts

k	iteration step
n	old time step
n + 1	Next time step

In recent years, many efforts have been made to model two-phase flow in a vertical channel using the DFM based on the advanced fully implicit method such as JFNK (Zou et al., 2016; Hajizadeh et al., 2017a,b; Hu et al., 2017). Based on these studies, one can conclude that using the JFNK method with an efficient preconditioner can lead to faster convergence and reduced computational cost. So far, these methods have not been widely applied to the reactor core thermal–hydraulic modeling using subchannel analysis. Downar and Joo (2001) investigate the application of preconditioned Krylov method for solving the two-phase flow continuity equations in the VIPRE-02. They found that a preconditioned Krylov method has a significant effect on the reduction of the CPU time and convergence rate of the two-phase flow equations. Therefore, in this study, the thermal–hydraulic performance of the annular fuel assembly is modeled using the subchannel method by efficient techniques.

2. Development of the subchannel program

Extensive efforts have been made in the last few decades to model the fuel assembly of light water reactors in transition conditions. A comparison with a set of experimental data has shown that subchannel analysis codes can predict thermo-hydraulic parameters accurately, Moorthi et al., (2018). For the two-phase flow modeling, the homogeneous model, two-fluid model, and the drift flux model are used. In different versions of COBRA (Wheeler et al., 1976), MATRA (Yoo et al., 1999) and VIPRE-01 (Stewart et al., 1983) the homogeneous model and in THERMIT (Kelly et al., 1981) the two-fluid model are used for two-phase flow modeling. In this paper, the DFM is used for thermal–hydraulic modeling of annular fuel assembly using subchannel analysis. The features and benefits of the DFM can be found in Ishii and Hibiki (2010). The following section presents the equations of mass, energy, and momentum of the two-phase flow for external channels, followed by a description of the required constitutive correlations.

2.1. Governing equations

In an annular fuel assembly, there are two types of channels. The first type is internal channels that are isolated from other channels and have no lateral connections to other channels. Therefore, transverse flow expressions are not considered for these channels. The second type is the external channels that are in communication with the other outer channels, and the mass, energy and, momentum exchange occurs along the channels. The external subchannel equations based on the DFM are as follows:

Mixture continuity equation:

$$\frac{\partial \rho_m}{\partial t}+\frac{\partial(\rho_m u_m)}{\partial z}+\frac{1}{A_i}\sum_k w_{ik}+\frac{1}{A_i}\sum_k (w'_{ik}-w'_{ik})=0 \tag{1}$$

Continuity equation for vapor phase:

$$\frac{\partial(\alpha\rho_g)}{\partial t}+\frac{\partial(\alpha\rho_g u_m)}{\partial z}+\frac{1}{A_i}\frac{(\alpha\rho_g)_i}{\rho_{mi}}\left(\sum_k w_{ik}+\sum_k (w'_{ik}-w'_{ki})\right) = \Gamma_g-\frac{\partial}{\partial z}\left(\frac{\alpha\rho_g\rho_l}{\rho_m}\overline{V_{gi}}\right) \tag{2}$$

Mixture enthalpy equation:

$$\frac{\partial(\rho_m h_m)}{\partial t}+\frac{\partial(\rho_m h_m u_m)}{\partial z}+\frac{1}{A_i}\sum_k w_{ik}h^*+\frac{1}{A_i}\sum_k (w'_{ik}h'_i-w'_{ki}h'_k) = -\frac{\partial}{\partial z}\left[\frac{\alpha\rho_g\rho_l}{\rho_m}\Delta h_{gl}\overline{V_{gi}}\right]+\sum_j \frac{q''_j\xi_{hj}}{A_{ij}}+\frac{\partial P}{\partial t} + \left[u_m+\frac{\alpha(\rho_l-\rho_g)}{\rho_m}\overline{V_{gi}}\right]\frac{\partial P}{\partial z} \tag{3}$$

Axial momentum equation:

$$\rho_m \frac{\partial u_m}{\partial t} + \rho_m u_m \frac{\partial u_m}{\partial z} + \frac{1}{A_i}\sum_k w_{ik} u^* + \frac{1}{A_i}\sum_k (w'_{ik} u'_i - w'_{ki} u'_k) = -\frac{\partial}{\partial z}\left[\frac{\alpha \rho_g \rho_l}{(1-\alpha)\rho_m}\overline{V_{gi}}^2\right] - \frac{\partial P}{\partial z} - \rho_m g - \left\{\frac{f_m}{D_h} + \frac{K}{\Delta z}\right\}\frac{\rho_m u_m |u_m|}{2} \quad (4)$$

Lateral Momentum equation:

$$\frac{\partial w_{ik}}{\partial t} + \frac{\partial w_{ik}\bar{u}_i}{\partial z} = \frac{s_{ik}}{L_c}(p_{ij} - p_{kj}) - K_{ik}\frac{w_{ik}|w_{ik}|}{2\rho^* s_{ik} L_c} \quad (5)$$

In the present study, the mixture momentum equation is used in the non-conservative form, because the errors generated are small, and it is simple for numerical implementation (Lee and Park, 2013). For the sake of simplification, some researchers (Talebi et al., 2012; Hashemi-Tilehnoee and Rahgoshay, 2013; Hajizadeh et al., 2017b) ignored the transverse momentum equation but in the subchannel analysis of annular fuels must be taken into account. In the above equations, h^* and u^* stand for the enthalpy and axial momentum, respectively transported by the diversion cross-flow. Typical values for h^* and u^* are:

$$\begin{aligned} w_{ik} > 0.0 \;&\rightarrow\; h^* = h_i, \quad u^* = u_i \\ w_{ik} < 0.0 \;&\rightarrow\; h^* = h_k, \quad u^* = u_k \end{aligned} \quad (6)$$

where k is the adjacent sub-channel to sub-channel i. The cross flow resistance coefficient K_{ik} consists of the frictional and the local pressure drop of the diversion cross flow, and its value is about 0.5 (Feng et al., 2007).

2.2. Constitutive relations

For closure of the system of equations, additional constitutive equations and equations of state for each phase are required. In this study, it is assumed that the vapor phase is saturated and the steam/liquid properties are determined from the IAPWS formulation 1995 (Wagner and Pruss, 2002).

The correlation of the Chexal and Lellouche (1986) is used to calculate the distribution parameter, C_0 and the mean drift velocity, $\overline{V_{gj}}$. These parameters indicate the effects of void distribution, and the relative velocity between the phases, respectively (Hibiki and Ishii, 2003). The Chexal-Lellouche model eliminates the need for two phase flow regime and covers a wide range of mass flux, pressure and channel size.

The distribution parameter and the mean drift velocity are given by:

$$C_0 = \frac{L}{K_0 + (1-K_0)\alpha^r} \quad (7)$$

and

$$\overline{V_{gj}} = 1.41\left(\frac{\Delta\rho g_z \sigma}{\rho_l^2}\right)^{1/4} C_2 C_3 C_4 C_9 \quad (8)$$

The constants C_2, C_3, C_4 and C_9 are defined by Chexal and Lellouche (1986).

The vapor generation term, in the RHS of Eq. (2), the vapor phase continuity equation is predicted by the constitutive relations as:

$$\Gamma_g = \Gamma_w + \Gamma_{ig} \quad (9)$$

where Γ_g has two regions: close to the wall and the bulk regions. For close to the wall region, the volumetric vapor generation rate is calculated by the Lahey model (Lahey, 1978):

$$\Gamma_w = \begin{cases} 0 & h_f < h_{cr} \\ \frac{q''_w a_w (h_f - h_{cr})}{(h_{f,sat} - h_{cr})(1+\varepsilon_p) h_{fg}} & h_{cr} \leqslant h_f \leqslant h_{f,sat} \\ \frac{q'''_w a_w}{h_{fg}} & h_f \geqslant h_{f,sat} \end{cases} \quad \text{where } \varepsilon_p = \frac{\rho_f\left[h_{f,sat} - \min(h_f, h_{f,sat})\right]}{\rho_g h_{fg}} \quad (10)$$

where

$$h_{cr} = \begin{cases} h_l^s - \frac{St.C_{pl}}{0.0065} & Pe > 70000 \\ h_l^s - \frac{Nu.C_{pl}}{455} & Pe \leqslant 70000 \end{cases} \quad (11)$$

The volumetric vapor generation rate in the bulk region is modeled by Eq. (12):

$$\Gamma_{ig} = \frac{H_{il}(T_l - T_{sat})}{h_{fg}} \quad (12)$$

In the present simulation, the RELAP5 (Fletcher and Schultz, 1992) flow map and correlations for a vertical boiling channel is used to obtain the liquid-to-interface volumetric interfacial heat transfer coefficients, H_{il}.

Constitutive correlations are needed to calculate the frictional pressure drop in single- and two-phase flows. In the single phase flow, the wall friction factor is the maximum value of the laminar (f = 64/Re) and turbulent (f = 0.32/$Re^{0.25}$) values. The two-phase frictional pressure drop is evaluated by the two-phase multiplier concept. In this approach, the two-phase pressure drop correlates to liquid-alone or vapor-alone pressure drop with a two-phase friction multiplier. In this paper, the two-phase friction multiplier is computed by the Armand correlation (Stewart et al., 1977).

In this paper, the actual quality is computed by the Levy model (Levy, 1967), heat transfer coefficient calculated from the Dittus-Boelter correlation (Dittus and Boelter, 1985) for single-phase flow and the Thom correlation for subcooled and saturated nuclear boiling (Collier and Thome, 1994).

3. Numerical solution methods

In this section, the computational schemes implemented in this study are briefly discussed. The finite volume method is applied to the spatial discretization of the governing equations on a staggered mesh, Fig. 1. The JFNK method is used to solve the discretized system of nonlinear equations. The appropriate flow distribution model and heat split model between the inner and outer channels were applied for the more accurate analysis of the dual-cooled annular fuel pins.

3.1. Fully implicit discretization of governing equations

By using the first-order upwind spatial discretization and the fully implicit backward Euler time integration scheme, discretization is carried out as follows:

Mixture continuity equation:

$$\Delta z \frac{(\rho^{n+1}_{mi,j} - \rho^n_{mi,j})}{\Delta t} + (\rho_m u_m)^{n+1}_{i,j+\frac{1}{2}} - (\rho_m u_m)^{n+1}_{i,j-\frac{1}{2}} + \frac{\Delta z}{A_i}\sum_{k\in i} w^{n+1}_{ik} + \frac{\Delta z}{A_i}\sum_{k\in i}(w'_{ik} - w'_{ik})^{n+1} = 0.0 \quad (13)$$

Continuity equation for the vapor phase:

$$\Delta z \frac{(\alpha\rho_g)^{n+1}_{i,j} - (\alpha\rho_g)^n_{i,j}}{\Delta t} + (\alpha\rho_g u_m)^{n+1}_{i,j+\frac{1}{2}} - (\alpha\rho_g u_m)^{n+1}_{i,j-\frac{1}{2}} + \frac{\Delta z}{A_i}\frac{(\alpha\rho_g)_{i,j}}{\rho_{mi,j}}\left(\sum_{k\in i} w_{ik} + \sum_{k\in i}(w'_{ik} - w'_{ik})\right)^{n+1} - \Gamma^{n+1}_{i,j}\Delta z + \left[\frac{\alpha\rho_g\rho_l}{\rho_m}\overline{V_{gi}}\right]^{n+1}_{i,j+\frac{1}{2}} - \left[\frac{\alpha\rho_g\rho_l}{\rho_m}\overline{V_{gi}}\right]^{n+1}_{i,j-\frac{1}{2}} = 0.0 \quad (14)$$

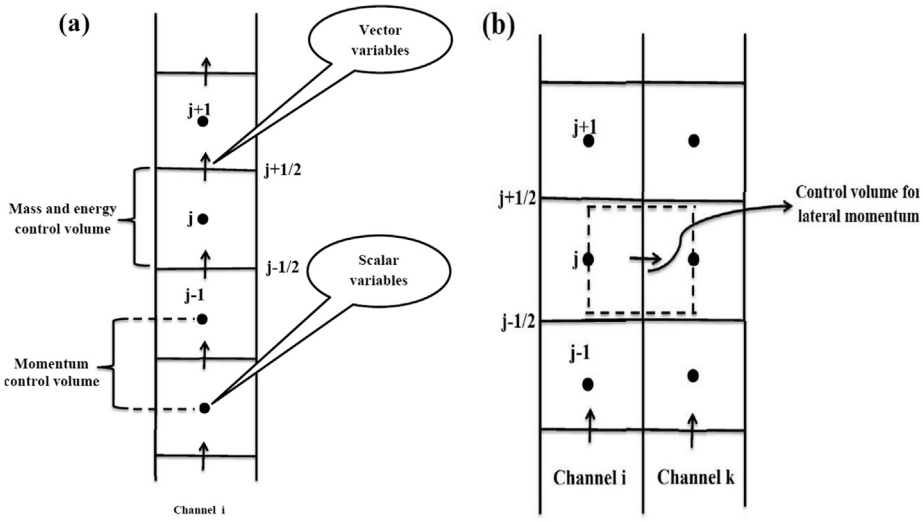

Fig. 1. Control volume for (a) axial and (b) lateral computational mesh.

Axial momentum equation:

$$\begin{aligned}&\Delta z\rho_{m_{i,j+\frac{1}{2}}}^{n+1}\frac{u_{m_{i,j+\frac{1}{2}}}^{n+1}-u_{m_{i,j+\frac{1}{2}}}^{n}}{\Delta t}+\rho_{m_{i,j+\frac{1}{2}}}^{n+1}u_{m_{i,j+\frac{1}{2}}}^{n+1}\left[u_{m_{i,j+1}}^{n+1}-u_{m_{ij}}^{n+1}\right]\\&+\left(P_{i,j+1}^{n+1}-P_{ij}^{n+1}\right)+\rho_{m_{i,j+\frac{1}{2}}}^{n+1}g_z\Delta z+\frac{1}{A_i}\left(\sum_{k\in i}w_{ik}u^{*}+\sum_{k\in i}(w'_{ik}u'_{i}-w'_{ki}u'_{k})\right)^{n+1}\\&+\left(\left(\frac{f_m}{D_h}+\frac{K}{\Delta z}\right)\frac{\Delta z}{2}\rho_m u_m|u_m|\right)_{i,j+\frac{1}{2}}^{n+1}+\left(\frac{\alpha\rho_g\rho_l}{(1-\alpha)\rho_m}\overline{V_{gi}}^{2}\right)_{i,j+1}^{n+1}\\&-\left(\frac{\alpha\rho_g\rho_l}{(1-\alpha)\rho_m}\overline{V_{gi}}^{2}\right)_{i,j-1}^{n+1}=0.0\end{aligned}\tag{15}$$

Mixture enthalpy-energy equation:

$$\begin{aligned}&\Delta z\frac{(\rho_m h_m)_{ij}^{n+1}-(\rho_m h_m)_{ij}^{n}}{\Delta t}+(\rho_m h_m u_m)_{i,j+\frac{1}{2}}^{n+1}-(\rho_m h_m u_m)_{i,j-\frac{1}{2}}^{n+1}\\&+\frac{1}{A_i}\left(\sum_{k\in i}w_{ik}h^{*}+\sum_{k\in i}\left(w'_{ik}h'_{i}-w'_{ki}h'_{k}\right)\right)^{n+1}\\&-\left[u_m+\frac{\alpha(\rho_l-\rho_g)}{\rho_m}\overline{V_{gi}}\right]_{i,j}^{n+1}\left(P_{i,j+\frac{1}{2}}^{n+1}-P_{i,j-\frac{1}{2}}^{n+1}\right)\\&-\Delta z\sum_{n\in i}\left(P_{wn,j}\Phi_{wn,j}q''_{wn,j}\right)^{n+1}-\frac{P_{ij}^{n+1}-P_{ij}^{n}}{\Delta t}\Delta z\\&+\left[\frac{\alpha\rho_g\rho_l}{\rho_m}\Delta h_{gl}\overline{V_{gi}}\right]_{i,j+\frac{1}{2}}^{n+1}-\left[\frac{\alpha\rho_g\rho_l}{\rho_m}\Delta h_{gl}\overline{V_{gi}}\right]_{i,j-\frac{1}{2}}^{n+1}=0.\end{aligned}\tag{16}$$

Lateral Momentum equation:

$$\begin{aligned}&\frac{\Delta z}{\Delta t}\left(w_{ik}^{n+1}-w_{ik}^{n}\right)+\left(w_{ikj}\bar{u}_{ij}\right)^{n+1}-\left(w_{ikj-1}\bar{u}_{ij-1}\right)^{n+1}\\&-\frac{s_{ik}\Delta z}{L_c}\left(p_{ij}^{n+1}-p_{kj}^{n+1}\right)+\frac{1}{2}\left(K_{ik}\frac{\Delta z v'}{s_{ik}L_c}\right)w_{ik}^{n+1}\left|w_{ik}^{n+1}\right|=0.0\end{aligned}\tag{17}$$

3.2. Jacobian-free Newton–Krylov methods

Eqs. (13)–(17) represents a system of nonlinear equations. The JFNK method is used to solve the discretized system of the nonlinear equations. This method has been widely used in many disciplines (Knoll and Keyes, 2004), and different fields such as geophysical flows (Reisner et al., 2001), two-phase flow (Ashrafizadeh et al., 2015; Pope and Mousseau, 2009), atmospheric flow (Reisner et al., 2003), hurricane model (Kurihara and Ross, 1993), shallow-water model (Mousseau et al., 2002), ice sheet model (Lemieux et al., 2011), ocean model (Bernsen et al., 2010), Plasma Physics (Mousseau and Knoll, 1997) and radiation diffusion (Mousseau et al., 2000).

In recent years, one of the topics in which the JFNK method has been widely used is the modeling of the nuclear reactor core. The nuclear reactor core is a complicate, multi-physical system in which highly nonlinear neutronic, thermal–hydraulic, and heat conduction equations are coupled together. Many attempts have been made to use the Newton-Krylov method to deal with the multi-physics coupling. Zhang et al. (2018a), solved the coupled neutronics/thermal-hydraulics equations in PWR core transient calculation. In this work, the Jacobin matrix is obtained analytically, and an incomplete LU factorization (ILU) scheme is used to precondition the Krylov solver GMRES. Knoll et al. (2011), presented a JFNK algorithm for k-eigenvalue/criticality calculations. In this study, they used the power iteration and Wielandt shift to construct a block preconditioner. Also, Mousseau (2006) developed more accurate algorithms for the simulation of a nuclear reactor by using the second order in time physics-based preconditioned JFNK method.

A brief description of the JFNK scheme to solve a set of nonlinear algebraic equations follows. Newton's method is used to solve the systems of nonlinear equations (Saad, 2003) of the form,

$$F(x)=0.\tag{18}$$

where **F** is the nonlinear residual for the unknown vector *x*. Newton's method solves Eq. (18) iteratively by solving a series of linear correction equations defined by:

$$J^{k}\delta x^{k}=-F(x^{k})\tag{19}$$

where

$$J_{i,j}(x^{k})=\frac{\partial F_i}{\partial x_j^{k}}\tag{20}$$

and

$$x^{k+1}=x^{k}+\delta x^{k}\tag{21}$$

The matrix *J* is the Jacobian matrix, the superscript k is the Newton iteration index and δx^{k} is the correction vector. The linear Eq. (19) is solved inexactly using the iterative Krylov solver GMRES (Saad and Schultz, 1986). The *m*th Krylov iteration is defined as follows:

$$x_m^{k}=x_0^{k}+a_0r_0+a_1Jr_0+a_2J^{2}r_0+\ldots+a_{m-1}J^{m-1}r_0\tag{22}$$

where

$$r_0 = J\delta x_0^k + F(x^k) \tag{23}$$

where δx_0^k is the initial guess of the linear solution. By using the pre-conditioner, the convergence of the GMRES algorithm is expected to be faster; therefore, to achieve a converged solution, fewer Krylov vectors are needed.

The computation and storage cost of the Jacobian coefficient matrix are significant and expensive for solving a large system of equations. One method to reduce the computational cost is to approximate the Jacobian matrix in Eq. (19) efficiently. In this procedure, the Jacobian matrix can be estimated by (Saad, 2003):

$$J^k v = \frac{F(x^k + \varepsilon v) - F(x^k)}{\varepsilon} \tag{24}$$

where ε can be formulated as (Pernice and Walker, 1998):

$$\varepsilon = \frac{\sqrt{(1 + \| u \|)\varepsilon_{mach}}}{\| \delta u_0 \|} \tag{25}$$

In this study, thermal hydraulic performance of annular fuels has been investigated, therefore, modifications for reducing the condition number of the Jacobian matrix such as scaling technologies (Zhang et al., 2018b; Park et al., 2010), do not have much effect on the performance of the JFNK method. Hence, scaling technologies are not used. To reduce the condition number of the Jacobian matrix and improve the convergence rate of the numerical methods, instead of solving the linear system in Eq. (19), equations are solved using the iterative Krylov solver restarted GMRES with a right preconditioning (Hu et al., 2017). Using the right preconditioner, Eq. (19) can be written as follows:

$$J^k P^{-1} P\ \delta x^k = -F(x^k) \tag{26}$$

where $\mathbf{P}$ is the preconditioner and actually $\mathbf{P^{-1}}$ estimates $\mathbf{J^{-1}}$; therefore, if $\mathbf{P} \approx \mathbf{J}$ ($\mathbf{P}$ is closer to $\mathbf{J}$), then solving the equations will be simpler. In this study, $\mathbf{P}$ is the preconditioning matrix that will be defined and constructed in the next section. The new matrix is now,

$$J'\ \delta x'^k = -F(x^k) \tag{27}$$

where

$$J' = JP^{-1} \tag{28}$$

and

$$\delta x' = P\ \delta x \tag{29}$$

Finally, the vector δx^k is calculated in an iterative process from the restarted GMRES solver as:

$$\delta x^k = P^{-1}\delta x'^k \tag{30}$$

There are several preconditioning procedures to the JFNK scheme discussed by Knoll and Keyes (2004). Lately, much attention has been paid to the physics-based preconditioner (PBP) and JFNK methods with PBP developed by some researchers. To solve the coupled boiling two-phase fluid and heat transfer problems, Mousseau (2004) employed the JFNK method with PBP. Mousseau stated that any solution scheme that linked with a reasonable estimation of a time step for the problem could be utilized as a preconditioner. A PBP can be obtained from the semi-implicit discretization of the governing equations (Elman et al., 2008). Hu et al. (2017) proposed the JFNK method with an efficient PBP for the 1-D subcooled boiling two-phase flow in a vertical channel. They showed that a PBP could be obtained from the semi-implicit temporal discretization of the governing equations for one-dimensional DFM. They concluded that the JFNK method for the 1-D subcooled flow boiling shows good robustness and accuracy.

An adequate selection of the PBP can considerably decrease the number of Krylov vectors, thus reducing both the storage requirement and the computational time. In this paper, PBP is used to precondition the Krylov solver GMRES. This method has been successfully applied for a vertical boiling channel modeling (Hu et al., 2017). We will now show in detail how to construct the pre-conditioner matrix, $\mathbf{P}$.

3.3. Construction of the preconditioner

Remember that the correction equation for Newton's method is defined as follows:

$$J\delta x = -F(x) \tag{31}$$

Usually, the linear discretization of the governing equations for a semi-implicit scheme on a staggered grid can be shown in the matrix form as:

$$Px = b \tag{32}$$

In this study, PBP is used, which requires to write the semi-implicit method compatible with Eq. (31) (Reisner et al., 2001, 2003, 2005; Mousseau et al., 2002). The "delta" form of the semi-implicit scheme is as:

$$P\delta x = -F(x) \tag{33}$$

Regardless of the transverse momentum equation (Downar and Joo, 2001) and employing the semi-implicit method on the staggered grid, the discretization of the governing equations used in the preconditioning for each channel is as follows:

$$\begin{aligned} F_{u_m,i,j+\frac{1}{2}} &= \Delta z \rho_{m\,i,j+\frac{1}{2}}^{n} \frac{u_{m\,i,j+\frac{1}{2}}^{n+1} - u_{m\,i,j+\frac{1}{2}}^{n}}{\Delta t} + \rho_{m\,i,j+\frac{1}{2}}^{n} u_{m\,i,j+\frac{1}{2}}^{n} \left[u_{m\,i,j+1}^{n} - u_{m\,i,j}^{n}\right] \\ &+ \left(P_{i,j+1}^{n+1} - P_{i,j}^{n+1}\right) + \frac{\Delta z}{A_i}\left(\sum_{k\in i} w_{ik} u^{*} + \sum_{k\in i}\left(w'_{ik}u'_{i} - w'_{ki}u'_{k}\right)\right)^{n} \\ &+ \left(\left(\frac{f_m}{D_h} + \frac{K}{\Delta z}\right)\frac{\Delta z}{2}\rho_m u_m |u_m|\right)_{i,j+\frac{1}{2}}^{n} \\ &+ \left\{\left(\frac{\alpha\rho_g\rho_l}{(1-\alpha)\rho_m}\overline{V_{gi}}^2\right)_{i,j+1}^{n} - \left(\frac{\alpha\rho_g\rho_l}{(1-\alpha)\rho_m}\overline{V_{gi}}^2\right)_{i,j-1}^{n}\right\} + \rho_{m\,i,j+\frac{1}{2}}^{n} g_z \Delta z \end{aligned} \tag{34}$$

$$\begin{aligned} F_{\rho_m,i,j} &= \frac{\rho_{m,i,j} - \rho_{m,i,j}^{n}}{\Delta t} + \left(\frac{\rho_m B}{\Delta z}\right)_{i,j-\frac{1}{2}}^{n} P_{i,j-1}^{n+1} - \left[\left(\frac{\rho_m B}{\Delta z}\right)_{i,j-\frac{1}{2}}^{n} + \left(\frac{\rho_m B}{\Delta z}\right)_{i,j+\frac{1}{2}}^{n}\right] P_{i,j}^{n+1} \\ &+ \left(\frac{\rho_m B}{\Delta z}\right)_{i,j+\frac{1}{2}}^{n} P_{i,j+1}^{n+1} + \left(\frac{\rho_m B}{\Delta z}\right)_{i,j+\frac{1}{2}}^{n} - \left(\frac{\rho_m B}{\Delta z}\right)_{i,j-\frac{1}{2}}^{n} \\ &+ \frac{\Delta z}{A_i}\sum_{k\in i} w_{ik}^{n} + \frac{\Delta z}{A_i}\sum_{k\in i}\left(w'_{ik} - w'_{ki}\right)^{n} \end{aligned} \tag{35}$$

$$\begin{aligned} F_{h_{m_{i,j}}} &= \Delta z \frac{(\rho_m h_m)_{i,j}^{n+1} - (\rho_m h_m)_{i,j}^{n}}{\Delta t} + (\rho_m h_m)_{i,j+\frac{1}{2}}^{n} (u_m)_{i,j+\frac{1}{2}}^{n+1} \\ &- (\rho_m h_m)_{i,j-\frac{1}{2}}^{n} (u_m)_{i,j-\frac{1}{2}}^{n+1} + \frac{\Delta z}{A_i}\left(\sum_{k\in i} w_{ik} h^{*} + \sum_{k\in i}\left(w'_{ki}h'_{k} - w'_{ik}h'_{i}\right)\right)^{n} \\ &- \left[u_m + \frac{\alpha(\rho_l - \rho_g)}{\rho_m}\overline{V_{gi}}\right]_{i,j}^{n}\left(P_{i,j+\frac{1}{2}}^{n+1} - P_{i,j-\frac{1}{2}}^{n+1}\right) - \Delta z \sum_{n\in i}\left(P_{wn,j}\Phi_{wn,j}q''_{wn,j}\right)^{n} \\ &- \frac{P_{i,j}^{n+1} - P_{i,j}^{n}}{\Delta t}\Delta z + \left[\frac{\alpha\rho_g\rho_l}{\rho_m}\Delta h_{gl}\overline{V_{gi}}\right]_{i,j+\frac{1}{2}}^{n} - \left[\frac{\alpha\rho_g\rho_l}{\rho_m}\Delta h_{gl}\overline{V_{gi}}\right]_{i,j-\frac{1}{2}}^{n} \end{aligned} \tag{36}$$

$$
\begin{aligned}
F_{\alpha,i,j} = {} & \Delta z \frac{\alpha_{i,j}^{n+1}-\alpha_{i,j}^{n}}{\Delta t} + \left(\frac{\Delta z \alpha}{\rho_g}\left(\frac{\partial \rho_g}{\partial P}\right)\right)_{i,j}^{n} \frac{P_{i,j}^{n+1}-P_{i,j}^{n}}{\Delta t} \\
& + \left(\frac{1}{\rho_g}\right)_{i,j}^{n}\left[(\alpha\rho_g)_{i,j+\frac{1}{2}}^{n} u_{m}{}_{i,j+\frac{1}{2}}^{n+1} - (\alpha\rho_g)_{i,j-\frac{1}{2}}^{n} u_{m}{}_{i,j-\frac{1}{2}}^{n+1}\right] \\
& + \frac{\Delta z}{A_i}\frac{\alpha_{i,j}^{n}}{\rho_{mi,j}^{n}}\left(\sum_{k\in i} w_{ik}^{n} + \sum_{k\in i}\left(w'_{ik} - w'_{ki}\right)^{n}\right) \\
& + \left[\frac{\alpha\rho_l}{\rho_m}\overline{V_{gi}}\right]_{i,j+\frac{1}{2}}^{n} - \left[\frac{\alpha\rho_l}{\rho_m}\overline{V_{gi}}\right]_{i,j-\frac{1}{2}}^{n} - \frac{\Gamma_{i,j}^{n}}{\rho_{gi,j}}\Delta z
\end{aligned}
\tag{37}
$$

where, the superscripts n and n + 1 represent the old and new time steps, and Δt is the time step size. In Eqs. (34)–(37), the convective terms and the pressure term in the continuity, momentum, and energy equations are evaluated at the new time level. In contrast, transverse flow and turbulent mixing terms, the enthalpy and axial momentum that transported by the diversion cross-flow (starred parameters), the wall friction term, and the wall heat source term are evaluated at the old-time level. These equations are obtained after substituting velocity correction equation, Eq. (38), into the mass equation and using the linear combination of mass and energy equations with simplifications.

$$
u_{m}{}_{i,j+\frac{1}{2}}^{n+1} = A_{i,j+\frac{1}{2}}^{n} + B_{i,j+\frac{1}{2}}^{n}\left(P_{i,j+1}^{n+1} - P_{i,j}^{n+1}\right) \tag{38}
$$

where

$$
A_{i,j+\frac{1}{2}}^{n} = u_{m}{}_{i,j+\frac{1}{2}}^{n} - \frac{\Delta t}{\Delta z \rho_{m}{}_{i,j+\frac{1}{2}}^{n}}\left[\begin{array}{l}
\rho_{m}{}_{i,j+\frac{1}{2}}^{n} u_{m}{}_{i,j+\frac{1}{2}}^{n}\left[u_{m}{}_{i,j+1}^{n} - u_{m}{}_{i,j}^{n}\right] \\
+\left(\left(\frac{f_m}{D_h}+\frac{K}{\Delta z}\right)\frac{\Delta z}{2}\rho_m u_m |u_m|\right)_{i,j+\frac{1}{2}}^{n} + \rho_{m}{}_{i,j+\frac{1}{2}}^{n} g_z \Delta z \\
+\left(\frac{\alpha\rho_g\rho_l}{(1-\alpha)\rho_m}\overline{V_{gi}}^{2}\right)_{i,j+1}^{n} - \left(\frac{\alpha\rho_g\rho_l}{(1-\alpha)\rho_m}\overline{V_{gi}}^{2}\right)_{i,j-1}^{n} \\
+\frac{1}{A_i}\left(\sum_{k\in i} w_{ik} u^{*} + \sum_{k\in i}\left(w'_{ik}u'_{i} - w'_{ki}u'_{k}\right)\right)^{n}
\end{array}\right] \tag{39}
$$

$$
B_{i,j+\frac{1}{2}}^{n} = -\frac{\Delta t}{\Delta z \rho_{m}{}_{i,j+\frac{1}{2}}^{n}} \tag{40}
$$

To write Eqs. (34)–(37) in a form analogous to Eq. (31), the following relations will be used:

$$
\delta u_{m\ i,j+\frac{1}{2}} = u_{m\ i,j+\frac{1}{2}}^{n+1} - u_{m\ i,j+\frac{1}{2}} \tag{41}
$$

$$
\delta P_{i,j} = P_{i,j}^{n+1} - P_{i,j} \tag{42}
$$

$$
\delta \alpha_{i,j} = \alpha_{i,j}^{n+1} - \alpha_{i,j} \tag{43}
$$

$$
\delta h_{m\ i,j} = h_{m\ i,j}^{n+1} - h_{m\ i,j} \tag{44}
$$

where $u_{m\ i,j+\frac{1}{2}}$, $P_{i,j}$, $\alpha_{i,j}$ and $h_{m\ i,j}$ in Eqs. (41)–(44) denotes the current solution of the linear equations. Eqs. (41)–(44) are substituted into Eqs. (34)–(37) to obtain the following equations:

$$
\rho_{m}{}_{i,j+\frac{1}{2}}^{n}\frac{\Delta z}{\Delta t}\delta u_{m,i,j+\frac{1}{2}} + \left(\delta P_{i,j+1} - \delta P_{i,j}\right) = -F_{u,m,i,j+\frac{1}{2}} \tag{45}
$$

$$
\left(\frac{\rho_m B}{\Delta z}\right)_{i,j-\frac{1}{2}}\delta P_{i,j-1} - \left[\left(\frac{\rho_m B}{\Delta z}\right)_{i,j-\frac{1}{2}} + \left(\frac{\rho_m B}{\Delta z}\right)_{i,j+\frac{1}{2}}\right]\delta P_{i,j} + \left(\frac{\rho_m B}{\Delta z}\right)_{i,j+\frac{1}{2}}\delta P_{i,j+1} = -F_{\rho,i,j} \tag{46}
$$

$$
\begin{aligned}
& \frac{1}{\Delta t}\left[h_{m,i,j}^{n}\left(\frac{\partial \rho_m}{\partial P}\right)_{i,j}^{n} - 1\right]\delta P_{i,j} + \frac{1}{\Delta t}\left[\rho_{m,i,j}^{n} + h_{m}{}_{i,j}^{n}\left(\frac{\partial \rho_m}{\partial h_m}\right)_{i,j}^{n}\right]\delta h_{m,i,j} \\
& + \frac{1}{\Delta z}(\rho_m h_m)_{i,j+\frac{1}{2}}^{n}\delta u_{mi,j+\frac{1}{2}} - \frac{1}{\Delta z}(\rho_m h_m)_{i,j-\frac{1}{2}}^{n}\delta u_{m,i,j-\frac{1}{2}} \\
& - \frac{1}{\Delta z}\left[u_m + \frac{\alpha(\rho_l-\rho_g)}{\rho_m}\overline{V_{gi}}\right]_{i,j}^{n}\left(\delta P_{i,j} - \delta P_{i,j-1}\right) = -F_{h,m,i,j}
\end{aligned}
\tag{47}
$$

$$
\begin{aligned}
& \frac{\Delta z}{\Delta t}\delta \alpha_{i,j} + \left(\frac{\alpha}{\rho_g}\left(\frac{\partial \rho_g}{\partial P}\right)\right)_{i,j}\frac{\Delta z}{\Delta t}\delta P_{i,j} + \left(\frac{1}{\rho_g}\right)_{i,j}(\alpha\rho_g)_{i,j+\frac{1}{2}}\delta u_{m,i,j+\frac{1}{2}} \\
& - \left(\frac{1}{\rho_g}\right)_{i,j}(\alpha\rho_g)_{i,j-\frac{1}{2}}\delta u_{m,i,j-\frac{1}{2}} = -F_{\alpha,i,j}
\end{aligned}
\tag{48}
$$

Because the delta form of the semi-implicit preconditioner is used, therefore, for each channel Eqs. (45)–(48) can be demonstrated in the vector form as:

$$
P\delta x = -F = -\left(F_{\rho,m,i,j}, F_{u,m,i,j+\frac{1}{2}}, F_{h,m,i,j}, F_{\alpha,i,j}\right)^{T} \tag{49}
$$

Eq. (49) is compatible with Eq. (31). As already mentioned, the coefficient matrix **P** in Eq. (49) is an approximation of the Jacobian matrix **J** in Eq. (31). Thus, the matrix **P** is employed for the preconditioning of the Jacobian matrix of Eq. (31). The detailed derivation of the components of the matrix **P** can be found in Appendix A.

3.4. Numerical solution scheme and flow distribution model

Fig. 2 shows the solution diagram. In this study, (1) the inlet temperature, (2) the inlet void fraction (usually $\alpha_g = 0$ at the inlet), (3) the output pressure, and (4) the inlet mass flow rate are applied as boundary conditions. The values of the initial-boundary condition parameters for the 13 × 13 fuel rod design benchmark calculation and sub-channel analysis are given in Tables 2 and 4, respectively.

Eqs. (45)–(48) can be solved by the semi-implicit numerical solution method (Liles and Reed, 1978; Talebi et al., 2012) and then use this solution as a preconditioner as well as the initial guess of the Newton-Krylov iterations. In this paper, to improve the numerical stability as well as the convergence rate of the JFNK method, at the beginning of each time step the semi-implicit PBP method is used as preconditioning. Also, at the first time step, the semi-implicit method is only used to obtain an appropriate initial guess for the Newton-Krylov iterations. In the next time steps, the results at the last time step are used as the initial guess.

The following steps are performed at each channel to apply the semi-implicit method as a preconditioner:

In the new time step, the coefficients and right hand side of Eqs. (45)–(48) from the values of the previous time step are calculated.

Tridiagonal pressure equation is solved to obtain the pressure distribution at each channel using a linear solver such as Krylov method or Tri-Diagonal Matrix Algorithm (TDMA).

Using the values obtained from pressure distribution, mixture velocity by Eq. (45) is calculated.

Using the new values of pressure and mixture velocity, h_m and α are calculated from Eqs. (47) and (48), respectively.

The newly updated vector δx, including $\delta u_{m\ i,j+\frac{1}{2}}$, $\delta P_{i,j}$, $\delta \alpha_{i,j}$ and $\delta h_{m\ i,j}$ are transferred to the Krylov solver GMRESAfter construction of the semi-implicit PBP, Eqs. (13)–(16) are then solved in a full-implicit manner. At this stage, the Eqs. (13)–(16) are solved channel-by-channel. That is, for each subchannel, the above equations are solved simultaneously along the channel for all the axial levels.

In this paper, only Eqs. (13)–(16) are fully implicitly solved for each channel, so for the construction of PBP consistent with these equations, the transverse momentum equation is neglected and the terms of the transverse flow are calculated in the previous time step (Downar and Joo, 2001). In the next step, for the external channels with new values obtained for pressure, enthalpy, vapor fraction, and axial flow rate for each cell, the transverse momentum equation is solved Plane-by-plane. In the plane-by-plane method, also called the level-by-level method, in contrast to the channel-by-channel method, the transverse momentum equation

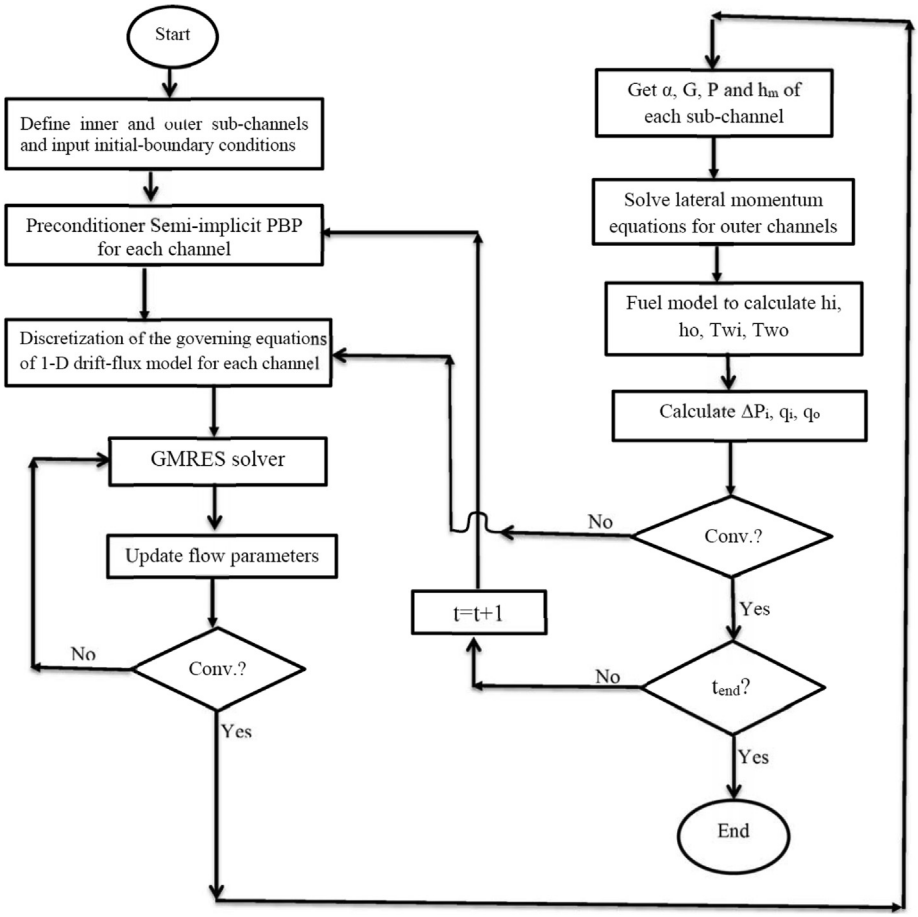

Fig. 2. Simplified flowchart of the calculation.

Table 1
Heat transfer fraction with different methods for the MIT 15 × 15 annular fuel design.

	Inner Chan.	Outer Chan.
Present method	38.6	61.4
SACAF (Xia et al., 2019)	38.8	61.2
THAF (Han and Chang, 2003)	38.4	61.6
RELAP5 (Han and Chang, 2003)	42.3	57.7

Table 2
Operating conditions for the 13 × 13 fuel rod design benchmark calculation.

Power	111 kW/m
Pressure	15.50 MPa
Coolant Flow Rate	0.78357 kg/s
Coolant Inlet Temp.	567.87 K
Gap conductance	6000 W/m^2–K
Axial Power Profile	Chopped Cosine (peak/average = 1.55)

is solved simultaneously at a defined axial level for all the external subchannels. The axial velocity terms at the higher level (j + 1) are computed from the old iteration step, and the terms at the lower levels are calculated from the new values of the solution at the current iteration step.

In the next step, using the annular fuel model developed by Esmaili et al. (2019), the temperature distribution inside the fuel, as well as the surface temperature of the fuel rod and the heat transfer coefficients between the clad and coolant are calculated. In the next step, after calculating the heat transfer fraction of each channel and the pressure drop between the internal and external channels, their convergence is investigated. If convergence is not achieved, then the fully implicit solution of the equations is used, and the process is repeated until convergence criteria is achieved (the error in the calculation of the flow distribution and the heat split is within the acceptable range of error levels). After convergence, the above calculations are repeated for the next time step until t_{final} is reached. It is worth mentioning that Eq. (49) is calculated only once at any time step, this means that, the preconditioning matrix P is calculated at the first Newton iteration only, or reused during other Newton iterations if needed.

For dual-cooled annular fuels, how the flow is distributed among the channels is of great importance and needs to be determined. The coolant flow distribution is such that it results in an

Table 3
Comparison of mass flow rates and pressure drops.

	Present method		VIPRE-01 (Feng et al., 2007)	
	Inner Chan.	Outer Chan.	Inner Chan.	Outer Chan.
Pressure Drop (kPa)	211.1	211.1	209.4	209.4
Mass Flow Rate (kg/s)	0.413	0.371	0.415	0.370

Table 4
Summary of the design data and correlations used in sub-channel analysis.

Parameter	Specifications
Fluid model	Drift Flux model
Model region	the hot fuel assembly with 1/8 symmetry, full axial length
Fuel rod outer diameter	1.5367 cm
Fuel rod inner diameter	0.8633 cm
Inner and outer cladding thickness	0.57 mm
Gap width	0.062 mm
Guide tube outer diameter	1.5367 cm
Active length	3.66 m
Pitch	1.651 cm
Number of channels	47 channels – see Fig. 7
Number of rods	26 rods –see Fig. 7
Power	6037.5 MWth
Axial power profile	Chopped cosine, peak-to-average ratio = 1.55
Radial power distribution	See Fig. 7
Hot Assembly Peaking	1.587
Hot Pin Radial Peaking	1.65
Core mass flow rate	26,550 kg/s
Core inlet temperature	294.7 °C
Form loss coefficient for mixing grids in outer channels	0.6
Inlet and outlet form loss coefficient	0.4 for inlet and 1.0 for outlet
Equations of state	IAPWS report
Two-phase mixing model	Equal-volume-exchange turbulent mixing with void drift (EVVD) model (Pang, 2014)
CHF correlation for inner channels	W-3S, Grid mixing factor = 0.0
CHF correlation for outer channels	W-3L, grid mixing factor 0.043, grid spacing factor 0.066, grid factor leading coefficient 0.986
Two-phase friction multiplier	Armand model (Stewart et al., 1977)
Heat transfer correlations	
Single-phase flow	Dittus–Boelter correlation (Dittus and Boelter, 1985)
Subcooled and saturated nuclear boiling	Thom correlation

equal pressure drop for all the subchannels. In this paper, the flow distribution model applied by Han and Chang (2003) is used. In this model, first, the pressure drop of each channel, as well as the mean pressure drop of all channels, is calculated. The total pressure drop for each channel consists of the acceleration pressure drop, the gravitational pressure drop, and the frictional pressure drop. For external channels, the pressure drop caused by the grid spacers is also considered. In the next step, the pressure drop of each channel is compared with the mean pressure drop, and their convergence is investigated. If the error of equal pressure drop across all channels were within the permissible range, the calculation would be moved to the next time step. Otherwise, the computation is repeated assuming a new flow distribution. This loop is repeated until it reaches a mass flow distribution that results in equal pressure drop across all channels.

3.5. Heat transfer fraction (Heat split model)

To find the heat split, thermal–hydraulic equations are first solved with an assumed heat flux. The temperature distribution inside the annular fuel is calculated by the orthogonal collocation method (OCM) (Esmaili et al., 2019) and then the heat transfer coefficients of the coolant are obtained. After that, the heat transferred to the inner and outer channels is calculated as follows:

$$q_{in} = h_i A_i (T_{wi} - T_{bi}) \tag{50}$$

$$q_{out} = h_o A_o (T_{wo} - T_{bo}) \tag{51}$$

where h_i and h_o are the heat transfer coefficient between the clad and coolant in the inner and outer channels, respectively. Also, T_w and T_b are the wall and fluid temperatures, respectively. Next, the convergence of q_{in} and q_{out} is examined. If the convergence criteria is achieved, the calculations will be moved to the next time step. Otherwise, the values of the parameters at this step will be used as the initial value for the next iteration. This process continues until convergence is achieved.

4. Verification of the code

To validate the present model, the numerical results of the MIT 15 × 15 annular fuel design (Fig. 3) modeling are compared with the results of THAF and RELAP5 code performed by Han and Chang (2003). In this study, the Korea Standard Nuclear Power Plant (KSNPP) was selected as the reference for the core operating conditions. In Figs. 4 and 5 axial distribution of the heat flux in the inner and outer surfaces of the annular fuel rod obtained from the

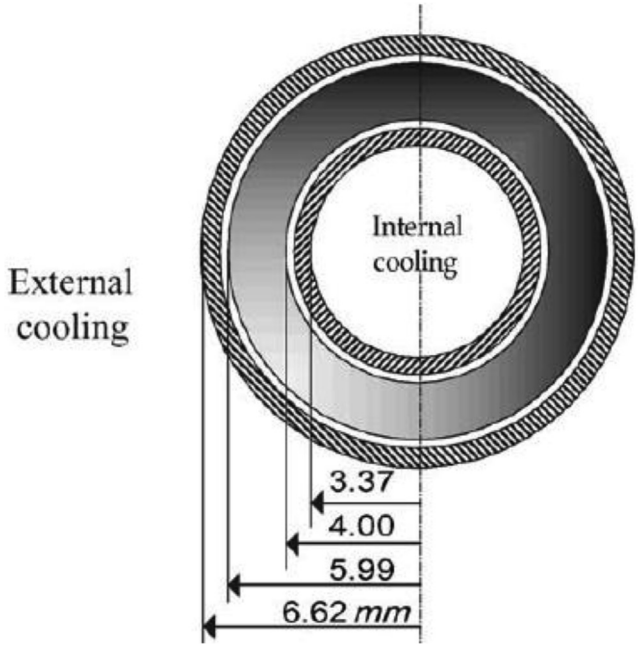

Fig. 3. Geometries in the 15 × 15 annular fuel unit cell.

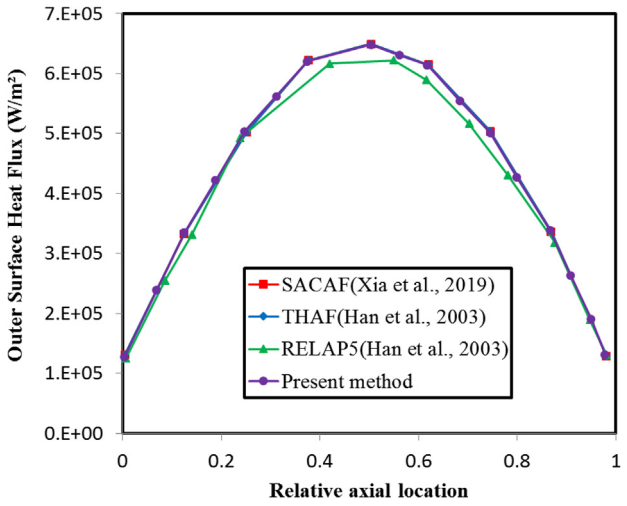

Fig. 4. Comparison of axial heat flux of the outer channel.

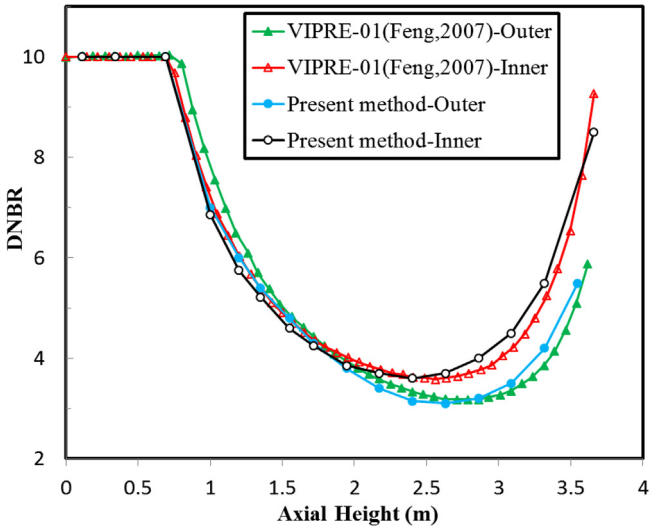

Fig. 6. Comparison of DNBR of the inner and outer channel.

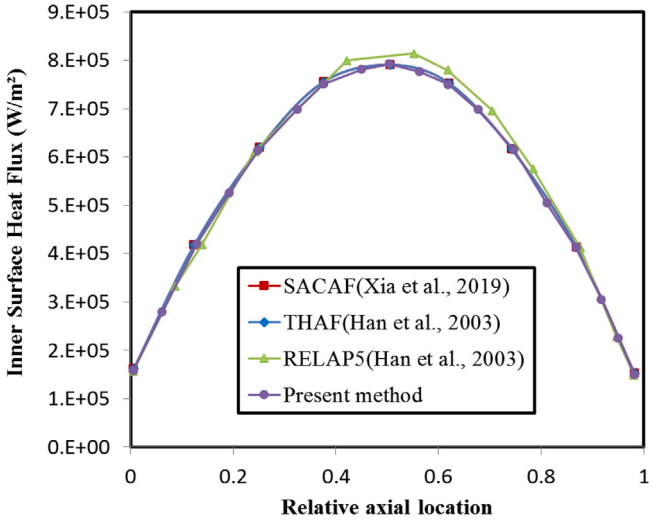

Fig. 5. Comparison of axial heat flux of the inner channel.

different methods is compared. Table 1 also presents the heat transfer fraction to the internal and external channels. The results show good agreement with different methods.

In this study, in addition to 15 × 15 annular fuel design, the results of the VIPRE-01 code (Feng et al., 2007) for the 13 × 13 arrays with the geometry and operation conditions shown in Table 2 is used in the validation. Table 3 compares the total pressure drop and mass flow rate obtained from the VIPRE-01 code and the present method. Comparing the results of Table 3 shows that the external channel has a higher pressure drop due to the grid spacers, but, the internal and external channel pressure drop must be the same, so less mass flow rate is driven toward the external channel. As seen in Table 3, the results are in good agreement with a difference of less than 1%.

A comparison of the DNBR profiles calculated by the present method and VIPRE-01 code along the internal and external channels using the W-3 CHF correlation is shown in Fig. 6. It can be seen from Fig. 6 that the results of the present methods and the VIPRE-01 code have small differences. The small differences are due to the application of different constitutive correlations, different two-phase flow models, as well as applying different thermodynamic properties of water/steam tables in each code.

5. Analysis of hot fuel assembly

In the core, due to the connection between the external channels and the transverse flow exchange, subchannel analysis of the hot fuel assembly is essential. In the following, the present method is applied to modeling the MIT 13 × 13 annular fuel assembly (Feng et al., 2007) operating at 150% power and flow rate using the parameters presented in Table 4. In this study, due to the symmetry and computational efficiency, 1/8 of the assembly is modeled. Fig. 7 illustrates the power distribution and numbering scheme of subchannels and rods in the hot fuel assembly. Summary of the design data and closure correlations used in subchannel analysis are given in Table 4 and Feng et al. (2007).

The axial distribution of the pressure drop in the hot inner and outer channels is shown in Fig. 8. As can be seen in the Fig. 8, the pressure drop variations in the internal channel are uniform, but for the outer channel, there are fluctuations due to the grid spacers. Fig. 8 shows that the results of the different methods are in good agreement. However, slight differences are due to the application of different correlations to calculate the pressure drop coefficients.

Table 5 compares the total pressure drop and MDNBR results obtained by the present method, and VIPRE-01 code for the hot fuel assembly. The results are in good agreement and the difference in total pressure drop and MDNBR values obtained by different methods is less than 2% and 5%, respectively. Table 5 shows that the MDNBR on the external channels is significantly larger than the internal channels. The reason will be discussed next.

Fig. 9 shows the comparison of the axial coolant temperature distribution in the internal and external channels. Also, Fig. 10 shows the axial distribution of the heat flux for the inner and outer surfaces of the hottest fuel rod. It can be seen that the cooling temperature in the outer channel is higher than that in the inner channel. This is due to the fact that, the hydraulic diameter of the inner channel is larger than that of the outer channel, as can be seen in Fig. 3 and Table 4, also the outer channel has a higher pressure drop due to the grid spacers, but the inner and outer channel pressure drop should be equal. Therefore, for the outer channel, the mass flow rate is lower. Furthermore, although the inner surface has a higher heat flux than the outer surface, most of the heat is transferred to the outer channel. Thus, the temperature of the outer channel is larger than that of the inner channel and reaches saturation temperature faster. The heat flux of the inner channel is

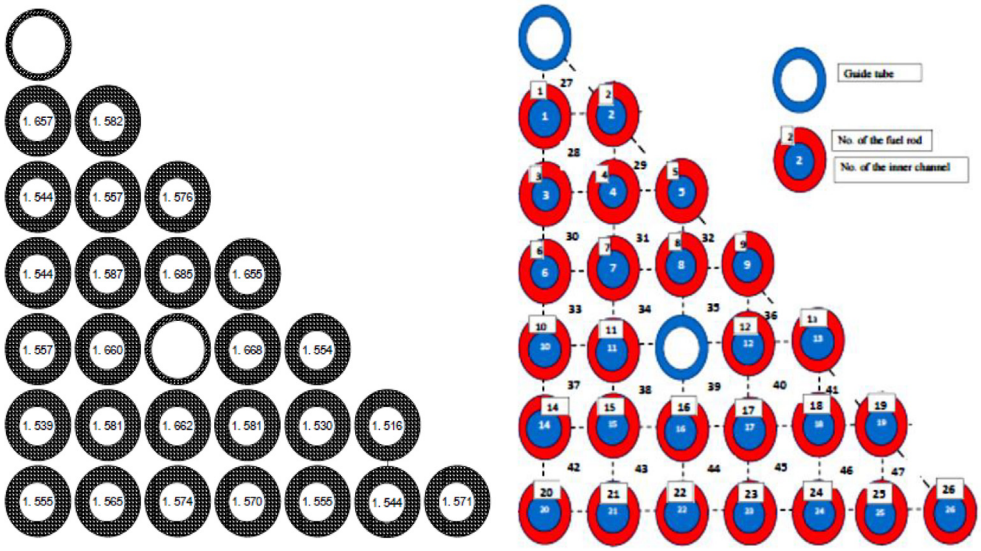

Fig. 7. Power distribution (left) and numbering scheme (right) in the hot fuel assembly with 1/8 symmetry.

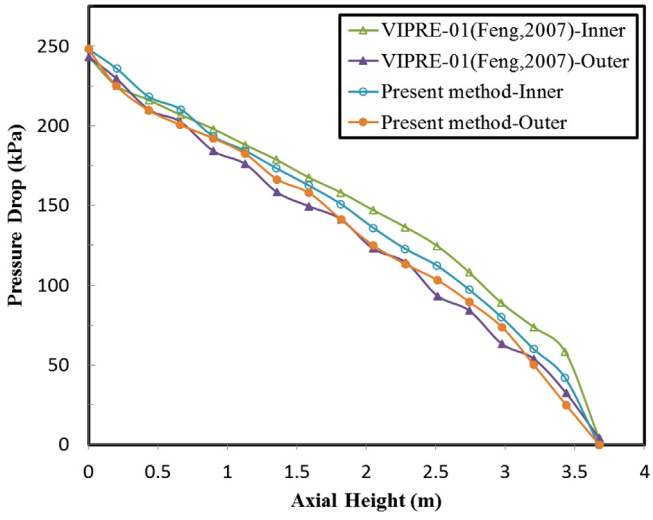

Fig. 8. Comparison of pressure drop in the inner and outer channel.

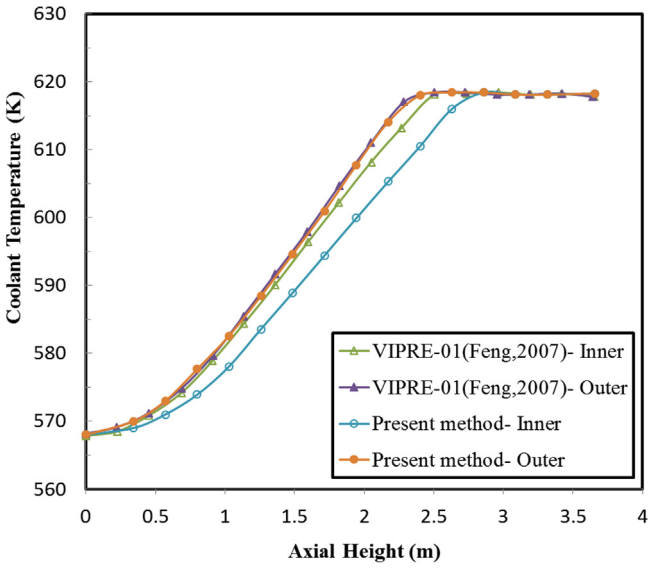

Fig. 9. Comparison of coolant temperatures in the hot inner and outer channels.

1.41 times that of the outer channel. This result is obtained when the internal and external gap conductance are equal ($h_{gi} = h_{go} = 6000$ W/m^2.K).

Fig. 11 illustrates the axial distribution of the mass flux in the inner and outer hot channel of the fuel assembly. In the inner channels, because of their isolation, the mass flux is constant along the channel and is higher than that of the outer channel. The mass flux for the outer hot channel is reduced due to the lateral flow along the channel, and the net flow to the hot channel is outward. The net outward flow of the outer hot channel is positive, because the thermal expansion of coolant reduces the density along the hot channel (Output lateral flow density is less than that of the input lateral flow) and the pressure drop reduces the flow rate along the heated channel. Therefore, the hot channel has a higher pressure drop due to the subcooled boiling along most of the length of the hot outer channel than the other channels. On the other hand, the boundary condition of equality of total pressure drop for all channels leads to a decrease in mass flux along the hot outer channel.

Fig. 12 shows the axial distribution of the void fraction versus equilibrium quality for the hot inner and outer channels of 13 × 13 annular fuel at 150% power. It is apparent that for the

Table 5
Comparison of the MDNBR and pressure drop results.

	Present method		VIPRE-01 (Feng et al., 2007)	
	Inner Chan.	Outer Chan.	Inner Chan.	Outer Chan.
MDNBR	1.45	2.04	1.37	1.93
Total pressure drop (MPa)	248		243	

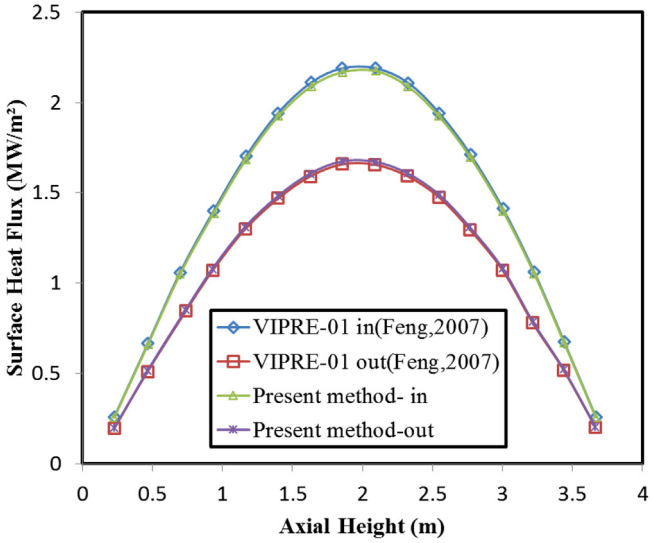

Fig. 10. Comparison of axial heat flux of the inner and outer channels.

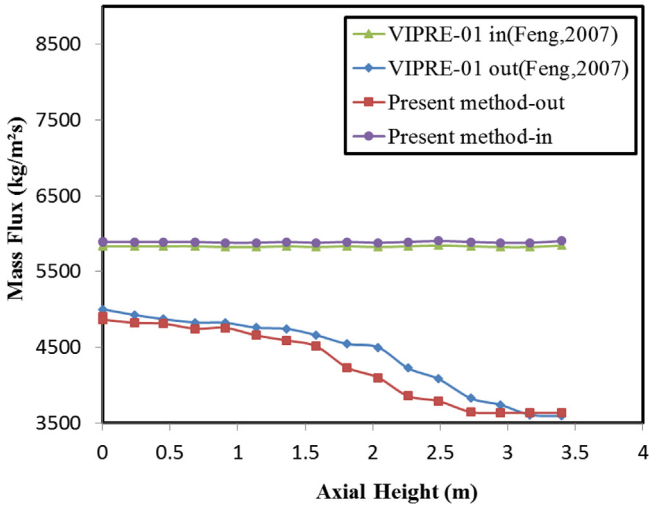

Fig. 11. Distribution of axial mass flux in the hot inner and outer channels.

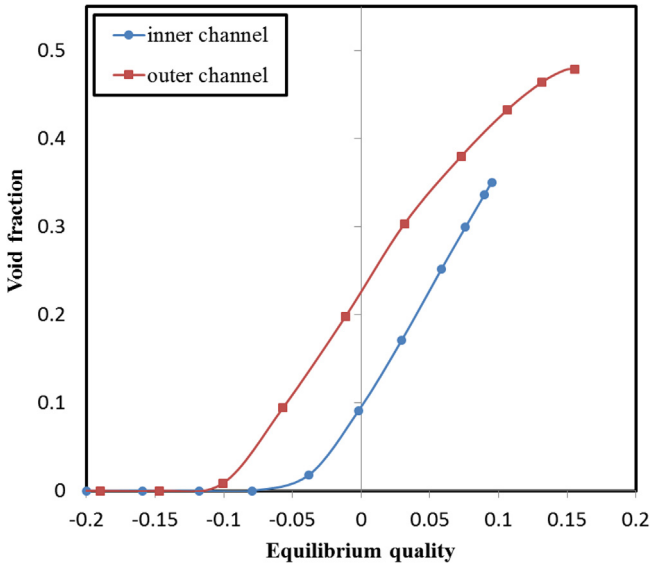

Fig. 12. Void fraction vs. quality profile in the hot inner and outer channels.

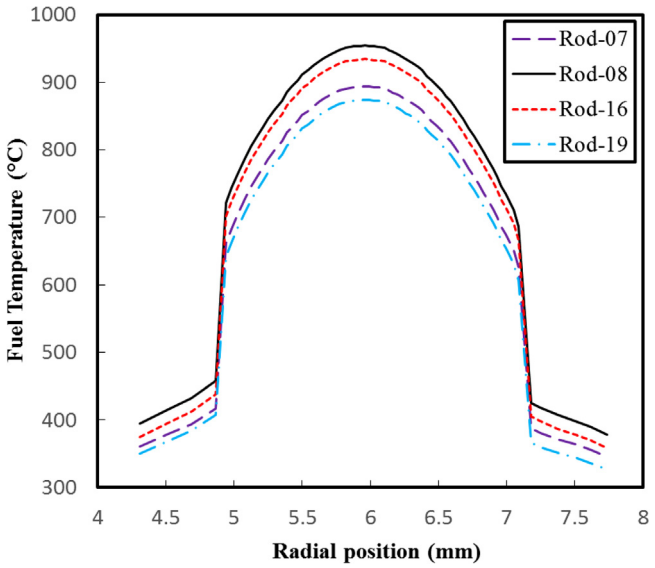

Fig. 13. Radial temperature distribution of some fuel rods.

hot outer channel, subcooled boiling started earlier, and the void fraction of the hot outer channel is higher than that of the hot inner channel. Because more of the heat transfer is directed to the outer channel. On the other hand, the mass flux of the outer channel is lower than that of the inner channel, and the coolant temperature in the outer channel is higher than that of the inner channel. Therefore, in the upper portion of the channel, the void fraction and equilibrium quality of the outer channel is higher than that of the inner channel.

The radial temperature distribution for the four annular fuel rods in the axial position where the maximum power is generated is shown in Fig. 13. It can be seen that due to the higher heat flux and larger power peaking factor, the temperature of the annular fuel rod, No. 8, is higher than the other rods.

Fig. 14 shows the axial distribution of the cooling temperature for four different rods. It is clear that the temperature of the outer channel is higher than the inner channel temperature due to more heat generation in the fuel pellet that is transmitted to the outer channel, and the lower mass flow of the outer channel than the inner channel.

Fig. 15 shows the axial distribution of the departure from nucleate boiling ratio (DNBR) for the NO. 8 and NO. 19 annular fuel rods using W-3 correlation. In annular fuel rods, the DNBR for the outer channel is higher than that of the inner channels. Due to the inter-channel mixing occurring in the outer channels, and the lower heat flux of the outer channels (DNBR = q''_{CHF}/q''_{actual}) the DNBR of the outer channels is higher than that of the inner channels which is consistent with the previous results.

To illustrate the benefits of annular fuels, the MDNBR results of the inner and outer channels of the MIT 13 × 13 annular fuel assembly operating at 150% power are compared with that of the hot channel of the reference solid fuel at 100% power (Feng et al., 2007) in Fig. 16. It can be seen that the results of the different methods are in good agreement, and the annular fuel has higher MDNBR than the solid fuel for most of the core length. Only at the end of the channel, the MDNBR of the annular fuel less is than that of the solid fuel, but it remains above the 1.3 limit.

Inlet and outlet temperatures and pressure of the annular fuel core are almost equal to the reference reactor, so the DNBR is mostly determined by the difference in mass flux and quality along

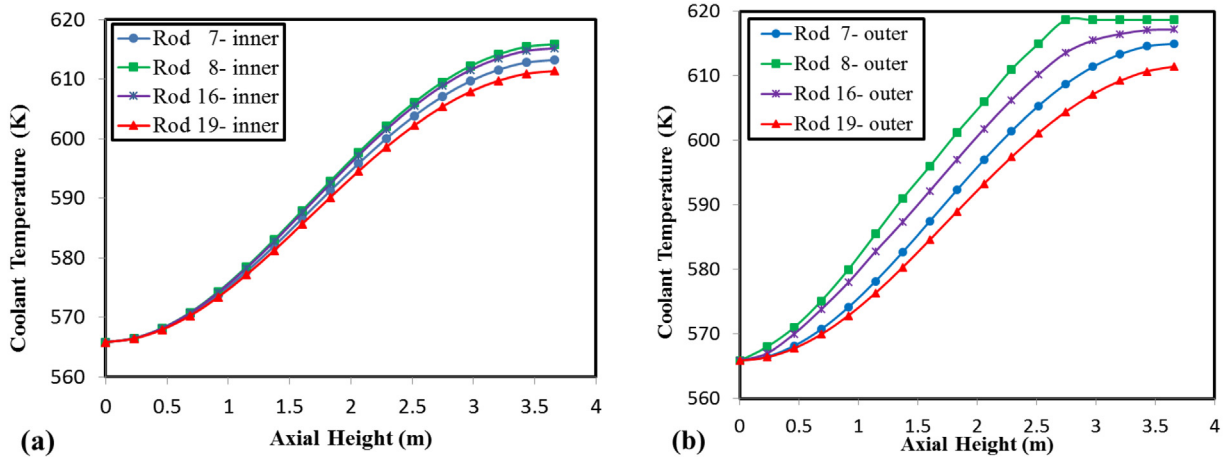

Fig. 14. Coolant temperature in the (a) inner and (b) outer channels of some rods.

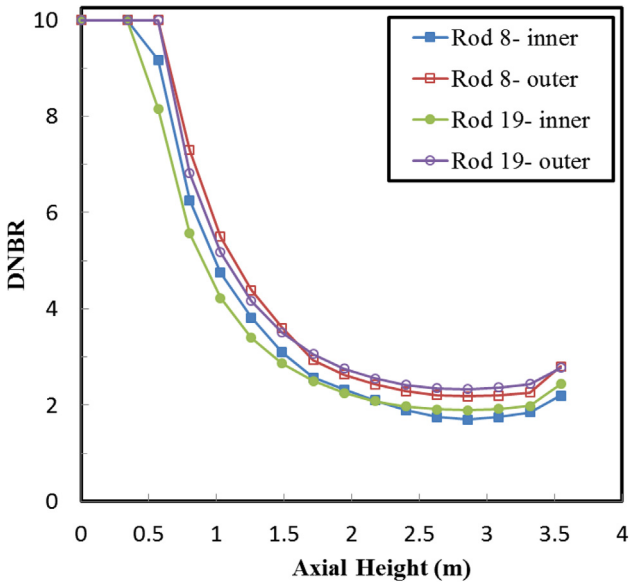

Fig. 15. DNBR of rod 8 and rod 19.

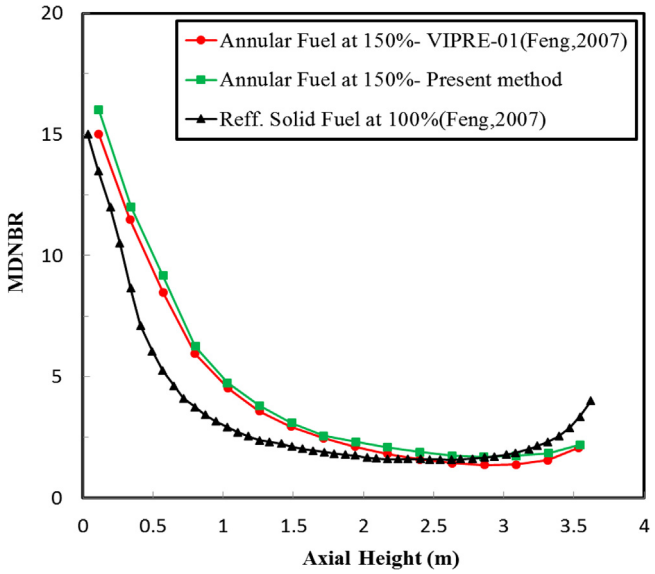

Fig. 16. Comparison of MDNBR of annular fuel and solid fuel.

the channels. At the lower section of the core, the cooling quality for the reference reactor and the annular fuel core are close. Therefore, the mass flux has more significant effect on the DNBR determination. The MIT 13 × 13 annular fuel core operating at 150% power also has 50% more mass flux, so its DNBR is higher. But at the upper section of the annular fuel core, as the cooling quality increases, the effect on the DNBR increases. The upper part of the annular fuel core has higher quality at 150% power, so the DNBR is reduced.

6. Conclusions

Modeling two-phase flow is a fundamental topic in terms of the safety and operation of nuclear reactors. Extensive research has been dedicated to the improvement of the current methods and models used for thermal–hydraulic simulations. In this study, a JFNK scheme with the semi-implicit PBP preconditioning was developed for the subchannel analysis of annular fuel assembly in a PWR based on the DFM. This study is the first successful application of the JFNK method with the semi-implicit PBP preconditioning for the subchannel analysis of the annular fuel assembly. The staggered grid finite volume method is used for spatial discretization, and the fully-implicit backward Euler time integration scheme is used for the temporal discretization of the governing equations.

Considerable emphasis is put on the verification of the present method by comparing the numerical results with the available data in the literature, for different arrays under different operating conditions, and reasonable agreement is observed. Differences between the computational results using different methods were also recognized and discussed. The following is the summary of the main findings:

(1) In the 13 × 13 annular fuel design, about 56% of the heat generated in the fuel is transferred to the outer channel and 44% to the inner channel. Therefore, the heat flux ratio of the inner wall to the outer wall is approximately 1.4.
(2) In the annular fuels, the mass flux of the inner channels remains constant due to the isolation and absence of the interchannel mixing. However, for outer channels, the mass flux varies along the channel due to the cross-flow (mixing effects) and the subcooled boiling along the channel.
(3) The inner channel has a higher mass flux than the outer channel due to the presence of the spacer grid on the outer channel.

(4) At the channel outlet of the 13 × 13 annular fuel operating at 150% power, the MDNBR is less than that of the reference solid fuel at 100% power. However, it remains above the 1.3 safety margin.
(5) A Comparison of the results showed that the JFNK method with a semi-implicit physics-based preconditioner can predict the subchannel parameters of the annular fuel assemblies with sufficient accuracy within 5%.

CRediT authorship contribution statement

H. Esmaili: Conceptualization, Methodology, Validation, Formal analysis, Investigation, Writing - original draft, Visualization. **H. Kazeminejad:** conceived the idea, involved in overall direction, planning and supervised the work. Contributed to the analysis of the results and to the writing and editing of the manuscript. **H. Khalafi:** Supervision. **S.M. Mirvakili:** Supervision.

Appendix A

Details of the preconditioning matrix

The block structure of the preconditioning matrix for channel i is as follow:

$$P=\begin{bmatrix} D^{P}_{\rho_m,i} & & & \\ L^{P}_{u_m,i} & D^{u_m}_{u_m,i} & & \\ L^{P}_{h_m,i} & L^{u_m}_{h_m,i} & D^{h_m}_{h_m,i} & \\ L^{P}_{\alpha,i} & L^{u_m}_{\alpha,i} & D^{\alpha}_{\alpha,i} \end{bmatrix} \tag{A.1}$$

Based on the discretized Eqs. (45)–(48), the components of the sub-block matrix can be determined as follows:

$$D^{P}_{\rho_m,i}(j,j-1)=\left(\frac{\rho_m B}{\Delta z}\right)^{n}_{i,j-\frac{1}{2}} \tag{A.2}$$

$$D^{P}_{\rho_m,i}(j,j)=-\left[\left(\frac{\rho_m B}{\Delta z}\right)^{n}_{i,j-\frac{1}{2}}+\left(\frac{\rho_m B}{\Delta z}\right)^{n}_{i,j+\frac{1}{2}}\right] \tag{A.3}$$

$$D^{P}_{\rho_m,i}(j,j+1)=\left(\frac{\rho_m B}{\Delta z}\right)^{n}_{i,j+\frac{1}{2}} \tag{A.4}$$

$$L^{P}_{u_m,i}(j,j+1)=1. \tag{A.5}$$

$$L^{P}_{u_m,i}(j,j)=-1. \tag{A.6}$$

$$D^{u_m}_{u_m,i}(j,j)=\rho_{m\,i,j+\frac{1}{2}}^{n}\frac{\Delta z}{\Delta t} \tag{A.7}$$

$$L^{P}_{h_m,i}(j,j-1)=\left(\frac{\rho_m h_m B}{\Delta z}\right)^{n}_{i,j-\frac{1}{2}}+\frac{1}{\Delta z}\left[u_m+\frac{\alpha(\rho_l-\rho_g)}{\rho_m}\overline{V_{gi}}\right]^{n}_{i,j} \tag{A.8}$$

$$L^{P}_{h_m,i}(j,j)=\frac{-1}{\Delta t}\left(1-h_m\left(\frac{\partial\rho_m}{\partial P}\right)\right)^{n}_{i,j}-\frac{1}{\Delta z}\left[u_m+\frac{\alpha(\rho_l-\rho_g)}{\rho_m}\overline{V_{gi}}\right]^{n}_{i,j} \tag{A.9}$$

$$L^{u_m}_{h_m,i}(j,j)=\left(\frac{\rho_m h_m}{\Delta z}\right)^{n}_{i,j+\frac{1}{2}} \tag{A.10}$$

$$L^{u_m}_{h_m,i}(j,j-1)=\left(\frac{\rho_m h_m}{\Delta z}\right)^{n}_{i,j-\frac{1}{2}} \tag{A.11}$$

$$D^{h_m}_{h_m,i}(j,j)=\frac{1}{\Delta t}\left[\rho_m+h_m\left(\frac{\partial\rho_m}{\partial h_m}\right)\right]^{n}_{i,j} \tag{A.12}$$

$$L^{P}_{\alpha,i}(j,j)=\left(\frac{\alpha}{\rho_g}\left(\frac{\partial\rho_g}{\partial P}\right)\right)^{n}_{i,j}\frac{\Delta z}{\Delta t} \tag{A.13}$$

$$L^{u_m}_{\alpha,i}(j,j-1)=-\left(\frac{1}{\rho_g}\right)^{n}_{i,j}\left(\alpha\rho_g\right)^{n}_{i,j-\frac{1}{2}} \tag{A.14}$$

$$L^{u_m}_{\alpha,i}(j,j)=\left(\frac{1}{\rho_g}\right)^{n}_{i,j}\left(\alpha\rho_g\right)^{n}_{i,j+\frac{1}{2}} \tag{A.15}$$

$$D^{\alpha}_{\alpha,i}(j,j)=\frac{\Delta z}{\Delta t} \tag{A.16}$$

where axial node number j = 1, N with N being the total number of control volumes in the vertical direction.

Appendix B. Supplementary data

Supplementary data to this article can be found online at https://doi.org/10.1016/j.anucene.2020.107616.

References

Ashrafizadeh, A., Devaud, C.B., Aydemir, N.U., 2015. A Jacobian-free Newton-Krylov method for thermal hydraulics simulations. Int. J. Numer. Meth Fluids.
Basile, D., Beghi, M., Chierici, R., Salina, E., Brega, E., 1999. COBRA-EN: An Upgraded Version of the COBRA-3C/MIT Code for Thermal Hydraulic Transient Analysis of Light Water Reactor Fuel Assemblies and Cores. Radiation Safety Information Computation.
Bernsen, E., Dijkstra, H.A., Thies, J., Wubs, F.W., 2010. The application of Jacobian-free Newton-Krylov methods to reduce the spin-up time of ocean general circulation models. J. Comput. Phys. 229 (21), 8167–8179.
Chexal, B., Lellouche, G., 1986. Full-range Drift-flux Correlation for Vertical Flows. Revision 1. Electric Power Research Inst..
Collier, J.G., Thome, J.R., 1994. Convective Boiling and Condensation. Clarendon Press.
Deng, Y., Wu, Y., Li, Y., Zhang, D., Tian, W., Su, G., Qiu, S., 2016. Mechanism study and theoretical simulation on heat split phenomenon in dual-cooled annular fuel element. Ann. Nucl. Energy 94, 44–54.
Deokule, A., Vishnoi, A., Dasgupta, A., Umasankari, K., Chandraker, D., Vijayan, P., 2014. Design and analysis of 19 pin annular fuel rod cluster for pressure tube type boiling water reactor. Nucl. Eng. Des. 276, 64–73.
Deokule, A., Vishnoi, A., Umasankari, K., Chandraker, D., Vijayan, P., 2015. Reactor physics and thermal hydraulic Analysis of annular fuel rod cluster for Advanced Heavy Water Reactor. Energy Procedia 71, 52–61.
Dittus, F., Boelter, L., 1985. Heat transfer in automobile radiators of the tubular type. Int. Commun. Heat Mass. 12 (1), 3–22.
Downar, T.J., Joo, H.G., 2001. A preconditioned Krylov method for solution of the multi-dimensional, two fluid hydrodynamics equations. Ann. Nucl. Energy 28 (12), 1251–1267.
Elman, H., Howle, V.E., Shadid, J., Shuttleworth, R., Tuminaro, R., 2008. A taxonomy and comparison of parallel block multi-level preconditioners for the incompressible Navier-Stokes equations. J. Comput. Phys. 227 (3), 1790–1808.
Esmaili, H., Kazeminejad, H., Khalafi, H., 2019. Prediction of temperature distribution in annular fuels using orthogonal collocation method. Ann. Nucl. Energy 134, 77–87.
Feng, D., Hejzlar, P., Kazimi, M.S., 2007. Thermal-hydraulic design of high-power-density annular fuel in PWRs. Nucl. Technol. 160 (1), 16–44.
Fletcher, C., Schultz, R., 1992. RELAP5/MOD3 Code Manual. Nuclear Regulatory Commission.
Hajizadeh, A., Kazeminejad, H., Talebi, S., 2017b. An advanced new fully implicit numerical method for two-phase flow subchannel analysis based on the Drift Flux Model. Ann. Nucl. Energy 108, 351–365.
Hajizadeh, A., Kazeminejad, H., Talebi, S., 2017a. A new numerical method for solution of boiling flow using combination of SIMPLE and Jacobian-free Newton-Krylov algorithms. Prog. Nucl. Energy 95, 48–60.
Han, K.H., Chang, S.H., 2003. Development of a thermal-hydraulic analysis code for annular fuel assemblies. Nucl. Eng. Des. 226 (3), 267–275.
Hashemi-Tilehnoee, M., Rahgoshay, M., 2013. Benchmarking a sub-channel program based on a drift-flux model with 8×8 NUPEC BWR rod bundle. Ann. Nucl. Energy 58, 202–212.
Hejzlar, P., Driscoll, M., Kazimi, M., 2001. Thermal hydraulics-I. 4. High-performance annular fuel for pressurized water reactors. Trans. Am. Nucl. Soc. 84, 192–194.

Hibiki, T., Ishii, M., 2003. One-dimensional drift-flux model and constitutive equations for relative motion between phases in various two-phase flow regimes. Int. J. Heat Mass Transfer 46 (25), 4935–4948.
Hu, L., Chen, D., Huang, Y., Li, X., Yuan, D., Wang, Y., 2017. JFNK method with a physics-based preconditioner for the fully implicit solution of one-dimensional drift-flux model in boiling two-phase flow. Appl. Therm. Eng. 116, 610–622.
Ishii, M., Hibiki, T., 2010. Thermo-fluid Dynamics of Two-phase Flow. Springer Science & Business Media.
Kelly, J., Kao, S., Kazimi, M.S., 1981. THERMIT-2: A Two-fluid Model for Light Water Reactor Subchannel Transient Analysis.
Knoll, D.A., Keyes, D.E., 2004. Jacobian-free Newton-Krylov methods: a survey of approaches and applications. J. Comput. Phys. 193 (2), 357–397.
Knoll, D.A., Park, H., Newman, C., 2011. Acceleration of k-eigenvalue/criticality calculations using the Jacobian-free Newton-Krylov method. Nucl. Sci. Eng. 167 (2), 133–140.
Kurihara, Y., Ross, R., 1993. An initialization scheme of hurricane models by vortex specification. Mon. Weather Rev. 121, 2030–2045.
Lahey Jr., R.T., 1978. A Mechanistic Subcooled Boiling Model. Library, Begel House Inc..
Lee, Y.G., Park, G.C., 2013. TAPINS: a thermal-hydraulic system code for transient analysis of a fully-passive integral PWR. Nucl. Eng. Technol. 45 (4), 439–458.
Lemieux, J.F., Price, S.F., Evans, K.J., Knoll, D., Salinger, A.G., Holland, D.M., Payne, A.J., 2011. Implementation of the Jacobian-free Newton-Krylov method for solving the first-order ice sheet momentum balance. J. Comput. Phys. 230 (17), 6531–6545.
Levy, S., 1967. Forced convection subcooled boiling-prediction of vapor volumetric fraction. Int. J. Heat Mass Transfer 10 (7), 951–965.
Liles, D., Reed, W.H., 1978. A semi-implicit method for two-phase fluid dynamics. J. Comput. Phys. 26 (3), 390–407.
Moorthi, A., Sharma, A.K., Velusamy, K., 2018. A review of sub-channel thermal hydraulic codes for nuclear reactor core and future directions. Nucl. Eng. Des. 332, 329–344.
Mousseau, V.A., 2004. Implicitly balanced solution of the two-phase flow equations coupled to nonlinear heat conduction. J. Comput. Phys. 200 (1), 104–132.
Mousseau, V.A., 2006. In: A Fully Implicit, Second Order in Time, Simulation of a Nuclear Reactor Core. American Society of Mechanical Engineers Digital Collection, pp. 383–392.
Mousseau, V.A., Knoll, D.A., 1997. Fully implicit kinetic solution of collisional plasmas. J. Comput. Phys. 136, 308–323.
Mousseau, V.A., Knoll, D., Rider, W., 2000. Physics based preconditioning and the Newton-Krylov method for non-equilibrium radiation diffusion. J. Comput. Phys. 160, 262–267.
Mousseau, V.A., Knoll, D., Reisner, J., 2002. An implicit nonlinearly consistent method for the two-dimensional shallow-water equations with Coriolis force. Mon. Weather Rev. 130 (11), 2611–2625.
Pang, B., 2014. Numerical Study of Void Drift in Rod Bundle with Subchannel and CFD Codes. KIT Scientific Publishing.
Park, H., Knoll, D.A., Gaston, D.R., Martineau, R.C., 2010. Tightly coupled multiphysics algorithms for pebble bed reactors. Nucl. Sci. Eng. 166 (2), 118–133.
Pernice, M., Walker, H.F., 1998. NITSOL: a Newton iterative solver for nonlinear systems. SIAM J Sci Comput 19 (1), 302–318.
Pope, M.A., Mousseau, V.A., 2009. Accuracy and efficiency of a coupled neutronics and thermal hydraulics model. Nucl. Eng. Technol. 41 (7), 885–892.
Reisner, J., Mousseau, V.A., Knoll, D., 2001. Application of the Newton-Krylov method to geophysical flows. Mon. Weather Rev. 129 (9), 2404–2415.
Reisner, J., Mousseau, A., Wyszogrodzki, A., Knoll, D., 2005. An implicitly balanced hurricane model with physics-based preconditioning. Mon. Weather Rev. 133 (4), 1003–1022.
Reisner, J.M., Wyszogrodzki, A.A., Mousseau, V.A., Knoll, D.A., 2003. An efficient physics-based preconditioner for the fully implicit solution of small-scale thermally driven atmospheric flows. J. Comput. Phys. 189 (1), 30–44.
Saad, Y., 2003. Iterative Methods for Sparse Linear Systems. SIAM.
Saad, Y., Schultz, M.H., 1986. GMRES: a generalized minimal residual algorithm for solving nonsymmetric linear systems. SIAM J. Sci. Stat. Comput. 7 (3), 856–869.
Shin, C.H., Chun, T.H., Oh, D.-S., In, W.K., 2012. Thermal hydraulic performance assessment of dual-cooled annular nuclear fuel for OPR-1000. Nucl. Eng. Des. 243, 291–300.
Stewart, C., Wheeler, C., Cena, R., McMonagle, C., Cuta, J., Trent, D., 1977. COBRA-IV: The Model and the Method. Pacific Northwest Lab, Richland, WA (USA).
Stewart, C., Cuta, J., Koontz, A., Kelly, J., Basehore, K., George, T., Rowe, D., 1983. VIPRE-01. A thermal-hydraulic analysis code for reactor cores. Volume 1. Mathematical modeling. Battelle Pacific Northwest Labs.
Talebi, S., Kazeminejad, H., Davilu, H., 2012. A numerical technique for analysis of transient two-phase flow in a vertical tube using the Drift Flux Model. Nucl. Eng. Des. 242, 316–322.
Vishnoi, A., Dasgupta, A., Chandraker, D., Vijayan, P., 2012. Development of analytical tools for thermal-hydraulics analysis of annular fuel assembly. Bhabha Atomic Research Centre.
Wagner, W., Pruss, A., 2002. The IAPWS formulation 1995 for the thermodynamic properties of ordinary water for general and scientific use. J. Phys. Chem. Ref. Data 31, 387–535.
Wheeler, C., Stewart, C., Cena, R., Rowe, D., Sutey, A., 1976. COBRA-IV-I: An Interim Version of COBRA for Thermal-hydraulic Analysis of Rod Bundle Nuclear Fuel Elements and Cores. Battelle Pacific Northwest Labs, Wash (USA) Richland.
Xia, H., Lu, C., Wu, Y., Wu, Z., Tian, W., Su, G., Qiu, S., 2019. Development of a subchannel analysis code and its application to annular fuel assemblies. Ann. Nucl. Energy 129, 428–436.
Xu, Z., Otsuka, Y., Hejzlar, P., Kazimi, M.S., Driscoll, M.J., 2007. High-performance annular fuel reactor physics and fuel management. Nucl. Technol. 160 (1), 63–79.
Yoo, Y.J., Hwang, D.H., Sohn, D.S., 1999. Development of a subchannel analysis code MATRA applicable to PWRs and ALWRs. J. Korean Nucl. Soc. 31 (3), 314–327.
Yuan, Y., 2004. The design of high power density annular fuel for LWRs PhD Thesis. Massachusetts Institute of Technology.
Zhang, Y., Cao, L., Liu, Z., Wu, H., 2018a. Newton-Krylov method with nodal coupling coefficient to solve the coupled neutronics/thermal-hydraulics equations in PWR transient analysis. Ann. Nucl. Energy 118, 220–234.
Zhang, H., Guo, J., Lu, J., Li, F., Xu, Y., Downar, T.J., 2018b. An assessment of coupling algorithms in HTR simulator TINTE. Nucl. Sci. Eng. 190 (3), 287–309.
Zou, L., Zhao, H., Zhang, H., 2016. Numerical implementation, verification and validation of two-phase flow four-equation drift flux model with Jacobian-free Newton-Krylov method. Ann. Nucl. Energy 87, 707–719.